PLOS ONE

RESEARCH ARTICLE

Synchrotron imaging and Markov Chain Monte Carlo reveal tooth mineralization patterns

Daniel R. Green[1,2]*, Gregory M. Green[3,4], Albert S. Colman[5], Felicitas B. Bidlack[2], Paul Tafforeau[6], Tanya M. Smith[1,7]

1 Department of Human Evolutionary Biology, Harvard University, Cambridge, Massachusetts, United States of America, **2** Forsyth Institute, Cambridge, Massachusetts, United States of America, **3** Physics Department, Stanford University, Palo Alto, California, United States of America, **4** Kavli Institute for Particle Physics and Cosmology, Stanford University, Palo Alto, California, United States of America, **5** Department of the Geophysical Sciences, University of Chicago, Chicago, Illinois, United States of America, **6** European Synchrotron Radiation Facility, Grenoble, France, **7** Australian Research Center for Human Evolution, Griffith University, Brisbane, Australia

* drgreen@fas.harvard.edu

Citation: Green DR, Green GM, Colman AS, Bidlack FB, Tafforeau P, Smith TM (2017) Synchrotron imaging and Markov Chain Monte Carlo reveal tooth mineralization patterns. PLoS ONE 12(10): e0186391. https://doi.org/10.1371/journal.pone.0186391

Editor: Siân E Halcrow, University of Otago, NEW ZEALAND

Received: April 3, 2017

Accepted: September 29, 2017

Published: October 19, 2017

Data Availability Statement: All relevant data are within the paper and its Supporting Information files.

Funding: This work was supported by National Science Foundation Grants 1247426 to DRG and 0923831 to ASC, the Wenner-Gren Foundation, the Leakey Foundation, Harvard University, and the European Synchrotron Radiation Facility award EC 1018 all to DRG.

Competing interests: The authors have declared that no competing interests exist.

Abstract

The progressive character of tooth formation records aspects of mammalian life history, diet, seasonal behavior and climate. Tooth mineralization occurs in two stages: secretion and maturation, which overlap to some degree. Despite decades of study, the spatial and temporal pattern of elemental incorporation during enamel mineralization remains poorly characterized. Here we use synchrotron X-ray microtomography and Markov Chain Monte Carlo sampling to estimate mineralization patterns from an ontogenetic series of sheep molars (n = 45 M1s, 18 M2s). We adopt a Bayesian approach that posits a general pattern of maturation estimated from individual- and population-level mineral density variation over time. This approach converts static images of mineral density into a dynamic model of mineralization, and demonstrates that enamel secretion and maturation waves advance at nonlinear rates with distinct geometries. While enamel secretion is ordered, maturation geometry varies within a population and appears to be driven by diffusive processes. Our model yields concrete expectations for the integration of physiological and environmental signals, which is of particular significance for paleoseasonality research. This study also provides an avenue for characterizing mineralization patterns in other taxa. Our synchrotron imaging data and model are available for application to multiple disciplines, including health, material science, and paleontological research.

Introduction

Teeth form incrementally, creating microscopic features that have been a subject of study since they were first observed by van Leeuwenhoek in the 17th century [1–4]. Tooth formation remains a focus of research today due to its relevance to material science, comparative and

evolutionary biology, and the reconstruction of health, diet, and seasonal climate patterns [5–10]. Enamel in particular is relevant to archeological and paleontological research because it is more resistant to postmortem chemical alteration than either dentin or cementum [6,11]. Enamel mineralization is traditionally conceptualized in two stages: secretion and maturation (S1 Text) [12–14]. While secretion is well characterized, maturation–when most mineral is incorporated–has been difficult to study and remains poorly understood [15–19], limiting applications in a variety of disciplines [20–30]. This study uses synchrotron density characterization to resolve uncertainty in the nature of enamel maturation, describing its timing and geometry, relationship to secretion, and variation within a population of animals.

Enamel formation begins when enamel-forming cells (ameloblasts) secrete a matrix of proteins and enzymes that control the formation of amorphous calcium phosphate (ACP) and its transformation into ordered hydroxyaparite (HAp) crystallites [12,13,23,31]. This process begins at the interface between enamel- and dentin-forming cells, where the future cusp will form. After initiation, the enamel secretory front advances towards the future cervix by successively activating neighboring ameloblasts, a process known as extension (Fig 1A). Simultaneously, these ameloblasts add organic matrix and mineral lattice from the enamel-dentin junction (EDJ) towards the enamel surface, thickening the enamel in a process known as apposition. Secreted enamel contains ordered daily and longer-period increments marking formation time (cross-striations and Retzius lines, respectively) [32–34], and accounts for 20–30% of mature mineral weight (10% volume) during its initial formation [13,17,35].

The majority of mineral is added during maturation, when ameloblast cells complete enamel secretion and rest on the surface of the tooth [13,14,36]. New vasculature is established by supporting ameloblasts, which change their ion channel and proteolytic enzyme production [13,14]. This increases ion concentrations to facilitate ACP and HAp formation [13,14]. Maturation has not been replicated *in vitro* and has been difficult to study *in vivo*. For this reason the spatial and temporal pattern of enamel mineralization remains contested and largely

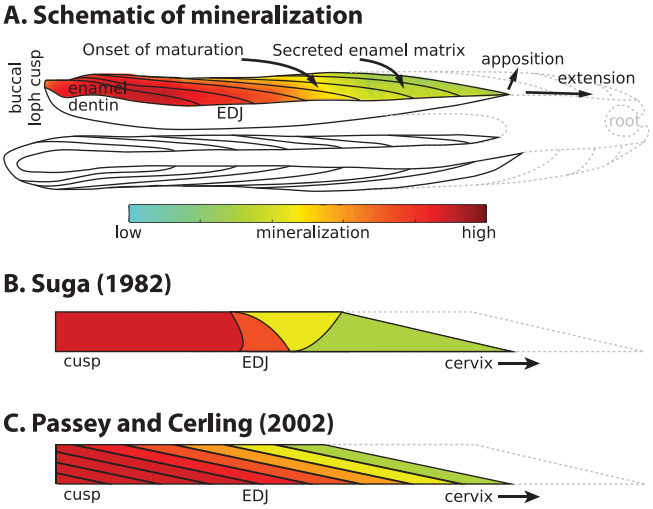

Fig 1. Models of enamel mineralization. (**A**) Growing sheep molar viewed in longitudinal section through lingual and buccal (colored) lophs. Mineralization initiates at the dentin horns (left) and proceeds towards the cervix (right) via extension and apposition until crown formation completes. Lines within enamel show incremental addition over time, and colors indicate maturation extent from low (green) to high (red). Solid lines represent formed enamel and dentin, while dotted lines depict future crown outlines. Schematic is based on the first molar (M1) enamel of a 14-week old animal from this study. (**B**) Mineralization model created by Suga (1982) [15] to represent maturation in large herbivore molars. (**C**) Mineralization model created by Passey and Cerling (2002) [17] to represent secretion and maturation in ever-growing teeth and tusks.

https://doi.org/10.1371/journal.pone.0186391.g001

unknown [5,15–19,34]. It is furthermore unclear when particular trace elements and ions are incorporated into enamel, and how tooth chemistry is modified by subsequent events during maturation [14,36]. The potential for "time averaging" complicates efforts to interpret the timing of physiological or environmental signals from enamel chemistry, as the prolonged and successive nature of maturation may overwrite the initial elemental record of secretion.

Two principle models have been proposed to explain the geometry and timing of maturation during mineralization. The first model was proposed by Shoichi Suga based on radiographs of primates and ungulates, and it describes a series of four waves of increasing mineralization moving to and from the EDJ through time [15,16,18,34] (Fig 1B). A second model by Ben Passey and Thure Cerling proposes that for ever-growing teeth, an initial secretory front is followed immediately by a single maturation wave in the same geometric orientation [17] (Fig 1C). This later model has been employed to estimate original body fluid isotope composition in an experimentally manipulated rabbit and domesticated sheep [5,37]. However, mineral density estimates from phosphorus concentration measurements, scanning electron microscopy and X-ray imaging reveal temporal pauses between mineralization phases of mammalian molars [15–19,34,38]. These density estimates show substantial heterogeneity in the spacing and geometry of maturation that is not accounted for in these models. This may be due to population-level variation, taxonomic differences, diffusion effects based on enamel thickness, or stochastic processes [18,19,34]. Furthermore, these models do not account for observed differences between enamel secretion and the geometry and propagation speed of maturation [15–19,34,38].

Here we address longstanding uncertainty in the timing and geometry of mineralization by constructing an empirical model describing ungulate molar mineralization over time. Our model is built from quantitative synchrotron X-ray microtomography (μCT) and Markov Chain Monte Carlo (MCMC) methods using the molars of sheep that died between the ages of 0–1.5 years old. We use sheep because of their established use as a model organism, and their enamel thickness and formation time broadly reflect patterns observed in large mammals, particularly herbivores used in paleoclimate reconstruction. Our method allows us to construct the first HAp-based dynamic picture of mineralization, including secretion and maturation phases, from discrete density measurements made from different individuals. This method differs from previous efforts to characterize mineralization in that it quantitatively reconstructs the timing, magnitude, and variation of mineralization over time in a population of animals.

Methods

Tooth samples

We dissected 45 first molars (M1s) and 18 second molars (M2s) from the mandibles of 45 Dorset sheep that died of natural causes between birth and 540 days of age (S1 Dataset). The animals were raised by the Cornell Sheep Program (Ithaca, NY) as part of a single breeding population. The study sample was balanced for sex: 53% were ewes and 47% rams. Adult Dorset sheep may live to eight years of age, though natural mortality is high in the first six months of life due to problems including birth trauma, starvation, or kidney stones. All teeth appeared free of significant pathology, and have been stored in 70% ethanol since the time of dissection.

Synchrotron imaging

The teeth were scanned on beamline ID17 of the European Synchrotron Radiation Facility (Grenoble, France) in two batches with an isotropic voxel size of 46μm. A second scan was conducted on a subset of teeth at higher resolution (13μm). We used synchrotron imaging because monochromatic X-ray beams with single energy values can be used to quantify

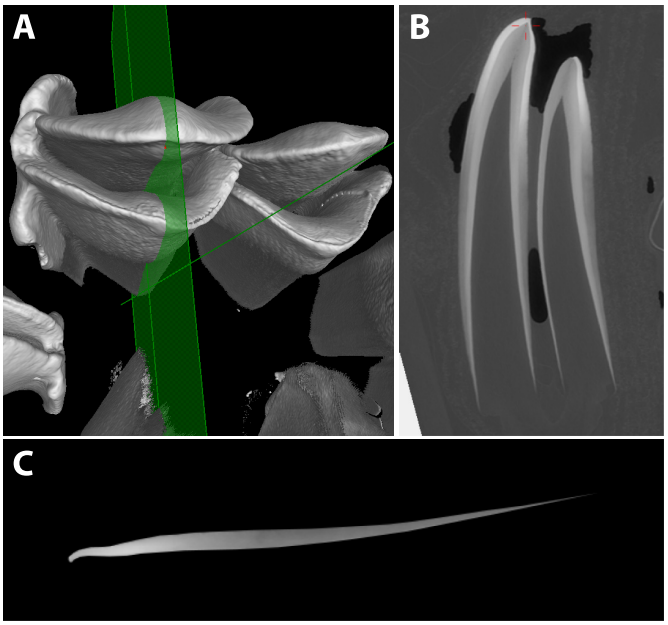

Fig 2. Virtual sectioning of sheep molars for model construction. (**A**) Synchrotron-scanned first molar with a bucco-lingual section plane. (**B**) Resulting section, with the cusp facing upward, lingual loph to the left, and buccal loph to the right. (**C**) Buccal enamel digitally extracted, with highest mineral density as the brightest shades of grey, and least density in darker shades. Pixel values were measured and converted into hydroxyapatite densities as detailed in the text.

https://doi.org/10.1371/journal.pone.0186391.g002

hydroxyapatite densities in mineralizing teeth [34]. In contrast, conventional μCT polychromatic beams with a complex mixture of X-ray energies are limited to qualitative density estimates [39,40]. Tomographic data were reconstructed using the PyHST2 ESRF software and monochromatic mode single distance phase retrieval to improve signal to noise [34] (detailed further in S2 Text). Molar lophs were virtually sectioned bucco-lingually with VGStudioMax 2.2 software, and the enamel was virtually extracted using Photoshop 5.0 (Fig 2).

HAp density values (ρ) from attenuation coefficients were calculated in grams of HAp per cubic centimeter from pixel grey values (Px) using the equations ρ = 6.9 x 10-5Px + 1.54 and ρ = 2.8 x 10-4Px + 1.49 for first and second sample scans, respectively [34,41]. To quantitatively compare enamel density values among teeth, we standardized spatial positions from each tooth with a uniform coordinate system defined by two coordinates: distance from the dentin horn along the EDJ, and distance from the EDJ to the tooth surface (S2 Text). For lightly-worn molars, the position of the dentin horn was estimated using unworn molars in the data set.

In order to model tooth growth over time, we used the EDJ length (degree of secretory-cell extension at death) and the age-at-death of each animal to calculate age as a sigmoid error function of enamel extension. When estimating extension curves, Gaussian rather than exponential or logistic functions were chosen based upon indications that highest extension rates are observed shortly after initiation [7, 42,43]. Fitting parameters of amplitude *a*, slope *s* and offset *o*, we used this function to re-assign size-modeled ages t_m to each section as a function of its extension length e_l, according to the equation

$$t_m = \frac{erf^{-1}((a + e_l - e_{lmax})/a) + (o^*s)}{s} \quad (1)$$

where erf^{-1} is the inverse error function, and e_{lmax} is the maximum length of the tooth when mature. Fitting of *a*, *o* and *s* for extension, maturation onset and completion was conducted

using the NLopt module for python, implementing the Multi-Level Single-Linkage (MLSL) and Constrained Optimization BY Linear Approximations (COBYLA) algorithms for global and local optimization, respectively [44,45].

Similar fitting curves were used to describe the average progress of maturation in the enamel crown. The onset and completion of maturation were defined as the estimated attainment of 40% and 85% HAp density midway between the EDJ and enamel surface, respectively, relative to the maximum measured density of 2.62g/cm^3 midway from the EDJ to the enamel surface. This is because mineralization data demonstrate that while trajectories are variable, all locations are either entering maturation phase with steep increases in mineral density (maturation onset), or leaving it with declines in mineral addition rate (maturation completion), at approximately 40% and 85% densities. To further validate our M1 and M2 extension modeling experimentally, we raised a single sheep for this study at the Harvard Concord Field Station. The animal received four 8mg/kg subcutaneous calcein injections, and was sacrificed by 180mg/kg IV sodium pentobarbital injection. Through polarized light and fluorescence microscopy, synchrotron imaging and dissection we determined M1 and M2 initiation times to be 49 days prior to and 84 days after birth, respectively. These values were employed for fitting extension and maturation curves (detailed further in S2 Text). Animal care and data collection protocols were approved by the Harvard University Faculty of Arts and Sciences Institutional Animal Care and Use Committee.

Mineralization model construction using MCMC method

To estimate mineral density increases for each location throughout the tooth crown we used an MCMC technique to sample from the Gaussian of likely mineralization histories given our observations for each coordinate in all teeth (detailed further in S2 Text). We assumed that HAp mineral density may only increase (minimum 10^{-5} g/cm^3 per sample time interval) in developing enamel:

$$L(\rho^d|\rho^m) = \prod_t \exp\left[-\frac{(\rho_t^m - \rho_t^d)^2}{2\sigma_t^2}\right] \quad (2)$$

where ρ^d and ρ^m are the measured and modeled pixel HAp densities over all time intervals t, ${\rho_t}^d$ and ${\rho_t}^m$ are the measured and modeled density for a particular time t, and σ_t is the estimated density error for each measurement. In these calculations we used a flat prior. Our model assumes that for a given pixel location density, measurements from each tooth are independent, and measurement error or natural biological variation amounts to 5% of all measurable HAp densities. In order to explore the posterior distribution of ρ^m, we employed Metropolis-Hastings with four walkers and 150,000 samples per pixel, of which we stored 100 for our model of tooth mineralization. The final model includes over 12,000 pixel locations, with density estimates calculated for 280 days per pixel (interpolating across measurements from each of 45 samples), and 100 density estimates per pixel-day (336 million density estimates).

Results

Synchrotron μCT imaging and tooth formation

Our virtual sections show maturation geometry is variable across individuals and times during formation (Fig 3). Enamel apposition and extension are also variable across the ontogenetic series, even though all animals derive from a single research population of high-percentage Dorset sheep (S1 Dataset). Though some of this variation may be attributed to obliquity of

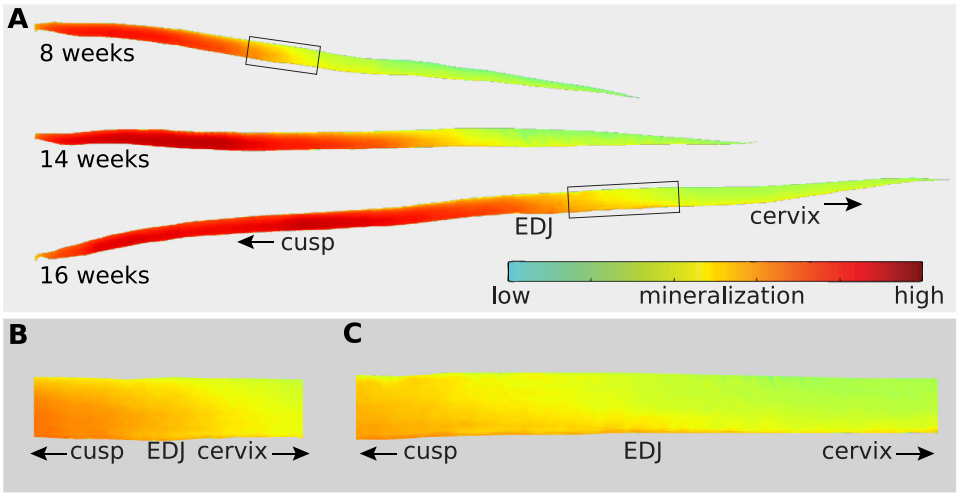

Fig 3. High-resolution (13μm) synchrotron scans of developing teeth reveal detailed density patterns. (**A**) Virtually dissected enamel crowns from molar scans of sheep that died at 8, 14 and 16 weeks of age. The gradient from red to green represent more to less HAp density, respectively. (**B**) Detail of maturation onset for the 8 week-old molar. (**C**) Detail of maturation onset for the 16 week-old molar, showing a more acute maturation geometry (orange and red boundary), with a highly mineralized innermost enamel layer leading in a cervical direction.

https://doi.org/10.1371/journal.pone.0186391.g003

virtual sections resulting from torsion in molar loph shape, much of observed shape variation is removed when a tooth coordinate system is used to standardize enamel shapes (Fig 4). At both low and high resolutions, flattened enamel scans clearly show separated secretion and maturation phases. These data suggest that despite general consistency in maturation timing

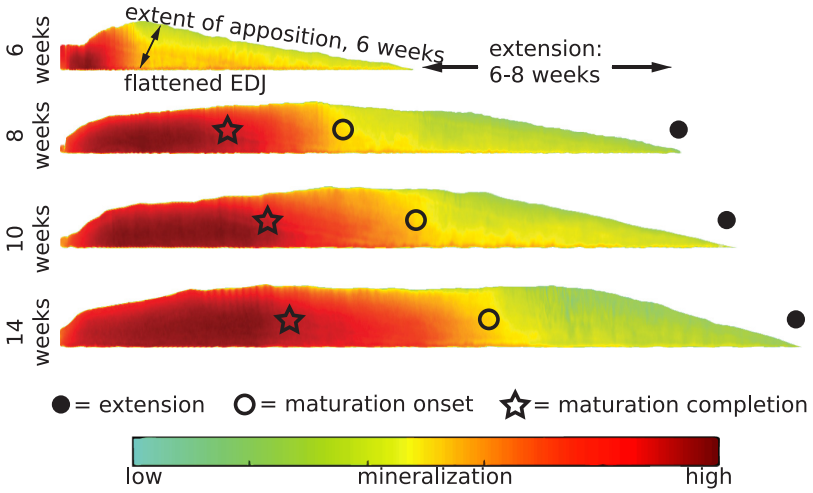

Fig 4. Shape standardization for quantitative comparisons between teeth. To compare mineralization among molar crowns at different developmental stages, sections are flattened along their enamel-dentin junctions (EDJs) and aligned. The progress of extension in each specimen is shown with black circles, the onset of maturation with open circles, and the completion of maturation with open stars. Maturation onset and completion are defined by the attainment of 40% and 85% mineral density, respectively, and their progress along the EDJ from the cusp (mm) was determined from a position halfway between the EDJ and enamel surface. Enamel maturation proceeds from an initial low HAp density (green) to a higher (red) density.

https://doi.org/10.1371/journal.pone.0186391.g004

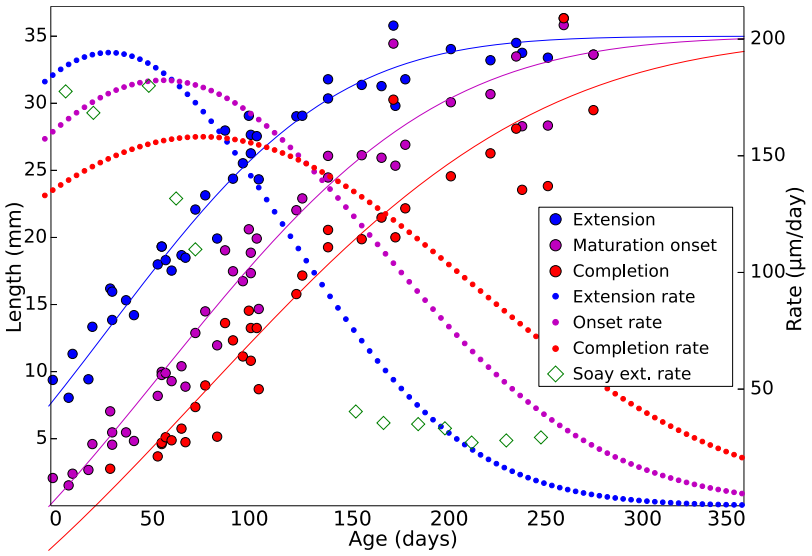

Fig 5. Gaussian modeling of extension and maturation for an ontogenetic series of sheep M1s. Measurements of enamel extension (blue circles), maturation onset (purple circles) and completion (red circles) start at the dentin horn tip (cusp) and proceed along the enamel-dentin junction (EDJ) from birth until the end of mineralization. Solid lines are fitted as integrated Gaussian functions. Published extension rates are also plotted from Soay sheep (green diamonds) [43], a more primitive breed than the Dorset sheep used here.

https://doi.org/10.1371/journal.pone.0186391.g005

and location, maturation geometry is more stochastic than secretion and likely driven by diffusive processes.

Gaussian modeling reveals that sheep first molars (M1s) rapidly extend in size around birth, with extension rates slowing between 100–150 days (Fig 5). Several M1s were nearly complete by 200 days of age. Decreasing postnatal extension rates are consistent with previous observations of sheep, bovid and equid M1s and third molars (M3s) [7,37,42,43,46]. We find that maturation onset and completion may also be modeled as a Gaussian process, with variation higher than that of extension only at the very latest time points. While extension rate peaks prior to maturation onset or completion rates, and achieves a higher maximum velocity, sustained late stage maturation velocity results in convergence with extension at the completion of mineralization.

MCMC mineralization model

By standardizing M1 shapes and assembling mineralization trajectories (S1 File) into a dynamic mineralization model (Fig 6), we find that secretion and maturation proceed in two waves that are distinct in geometry and timing (Fig 7; S2 File). Initial secretion occurs at a steep angle to the EDJ that becomes more oblique through time, while maturation occurs over a larger spatial area and longer time period, with a variable orientation largely perpendicular to the EDJ. Near the innermost enamel layer, sharp increases of mineral density during maturation occur after a pause that follows secretion. Significant mineral density increase occurs only after ameloblasts have completed secretion. Thus the time averaging of chemical input depends on the precise location within the crown. We can estimate this averaging at any given location within the tooth by observing the onset of secretion and the completion of maturation in the model mineralization trajectories (Fig 6). At most locations throughout the enamel, the total time averaged during mineralization is approximately 75–100 days. Locations at or near

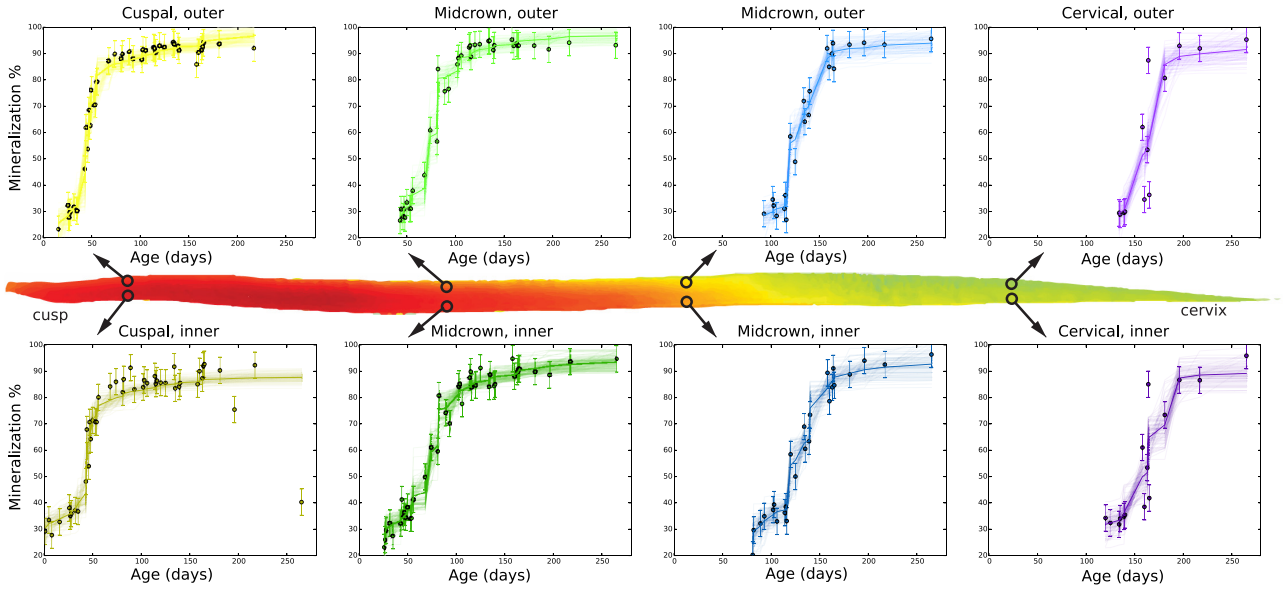

Fig 6. Mineralization percent over time (circles) determined from quantitative X-ray imaging. Mineralization trajectories (lines) were sampled at over 12,000 locations, of which eight are shown here. Cuspal enamel begins mineralizing earlier than cervical enamel and matures over a shorter time. After secretion, the enamel near the EDJ matures more slowly, while outer enamel farther from the EDJ proceeds from secretion to maturation more quickly and takes less time to mineralize overall.

https://doi.org/10.1371/journal.pone.0186391.g006

the surface enamel involve less time averaging (55–75 days). Once secretion has occurred near the enamel surface it is quickly followed by maturation.

This mineralization model is accessible in an HDF5 data format that can be adapted to a variety of purposes (S1 File).

Discussion

Relationship to previous enamel mineralization models

Suga [15] proposed that enamel maturation follows secretion after a pause, and occurs in a series of discontinuous waves with differing geometries. Passey and Cerling [17] proposed a simplified scenario for ever-growing teeth in which maturation is continuous with secretion, maintains the same geometry, and is invariant in intensity. Our results show that enamel secretion and maturation are discontinuous, and that the geometries of both phases are distinct (Fig 7). These data provide further evidence that herbivore molar extension and maturation rates are nonlinear, peaking shortly after initiation and slowly declining thereafter [7,37,42,43,46]. Our modeling does not support the presence of multiple maturation waves. Instead, it indicates that a single, primary maturation wave is followed by a minor density increase over a prolonged period. While the maturation geometry varies among individuals and at different times during formation (Fig 3), a robust temporal and spatial pattern of maturation is apparent (Fig 7; S2 File).

The consistency of this pattern is striking given the independent calculation of over 12,000 mineralization trajectories that each contribute to the model (Fig 6, S1 and S2 Files). Our observations produce a picture of mineralization distinct from the two available models [15–17], but consistent with ameloblast activity during secretion and maturation. During the initial phase ameloblasts secrete an array of structural and matrix-modifying proteins to stabilize a partially-mineralized scaffold, while simultaneously expanding it to establish what will become the mature enamel shape [2,3,6,12–14,33]. It is not until this process has completed that

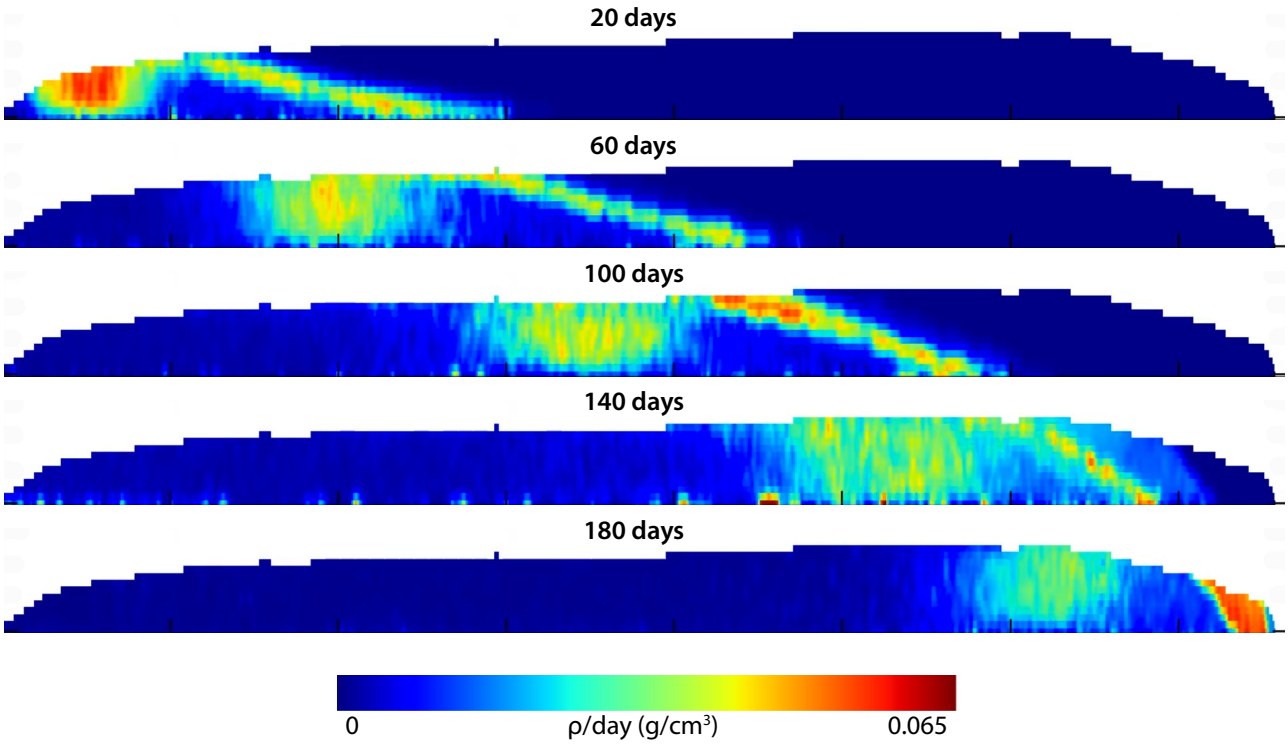

Fig 7. Mineralization density increases over time after assembling all synchrotron images into a single dynamic mineralization model. Mineral density increases from early (above) to successively later (below) stages of mineralization, shown with rapid density increases in warm colors, and no mineral density increase in dark blue. Dark blue color to the right of the secretory front shows future enamel that does not yet exist, and to the left of the maturation wave, enamel which has completed mineralization. The model shows that secretion is brief, occurs at a steep angle to the EDJ, and initially outpaces maturation. Maturation has a more diffuse geometry, follows secretion after a pause, and converges with secretion at the end of the mineralization process.

https://doi.org/10.1371/journal.pone.0186391.g007

ameloblasts structurally transform, ceasing mineral forming activity for a brief period, and begin to construct the ion channels that will be critical for driving up mineral concentrations and HAp density within the immature matrix [13,14]. From this point forward this ion channel activity, cleavage and clearing of structural proteins, and ameloblast-mediated pH fluctuations increase enamel mineral density while preserving ameloblast homeostasis [13,14, 47,48]

The implications for reconstructing body and environmental chemistry are best understood by comparing the predicted timing of secretory and maturational mineral deposition of the current and earlier models (Fig 8). In all models, enamel secretion is nearly instantaneous, while the timing of maturation differs. The chemical history will therefore manifest differently under each model, based upon the co-occurrence of inputs and mineral deposition phases at different locations throughout the enamel. Importantly, our results show that the separation between secretion and maturation is variable at different locations in the enamel crown. During initial formation of the cusp tip, maturation follows secretion after a pause. This pause is more brief near the enamel surface. Later in tooth formation, the maturation wave is more or less continuous with secretion. The implications for different applications are below.

Implications for health, paleontology, and biomineralization

This method can be used to model the mineralization of human teeth, for which many aspects of mineral incorporation remain unknown. An empirical model of mineral density changes can provide a framework for interpreting the etiology of enamel defects that are typically

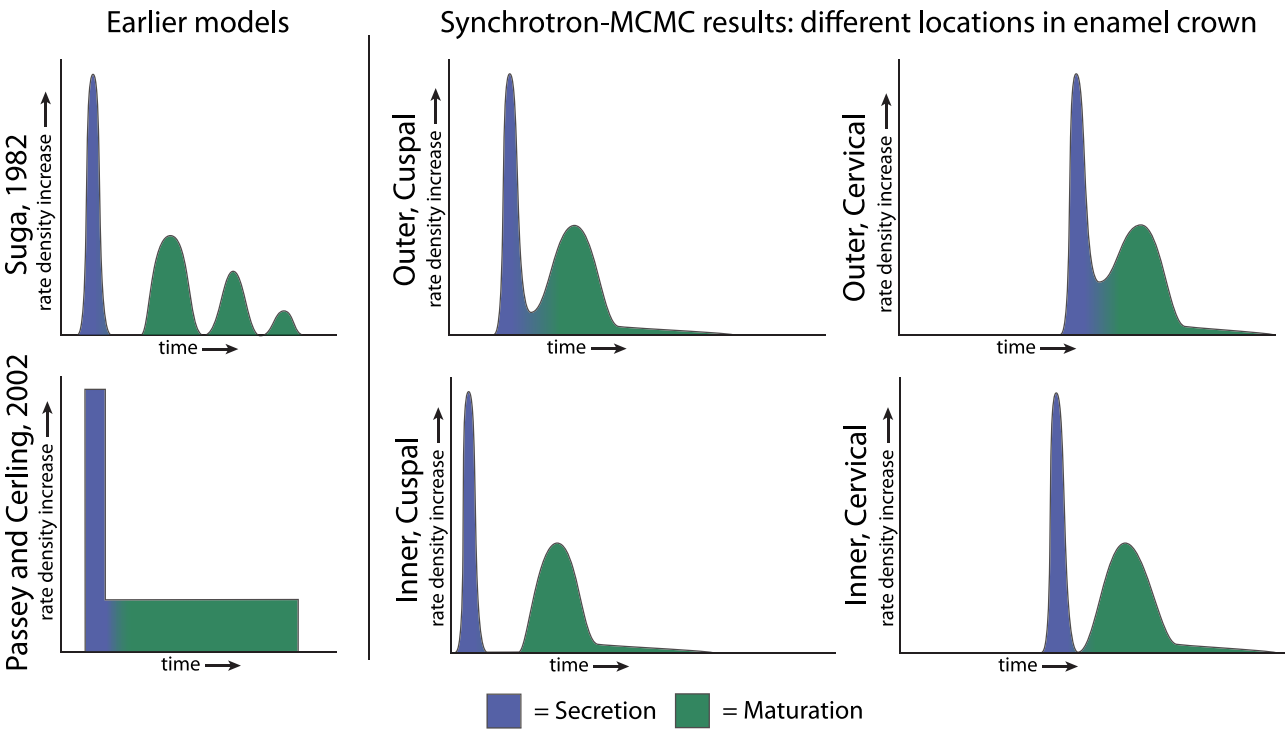

Fig 8. Schematic of mineral deposition rate over time. Mineral deposition over time in published models (left) and as found in this study (center and right), with secretion in purple, and maturation in green. In the Suga (1982) model, maturation is not continuous with secretion and is broken into a series of waves (top left). In the model of Passey and Cerling (2002) both mineralization phases are contiguous and maturation is constant. We find that secretion and maturation are discontinuous cuspally (center), less so near the enamel surface (above) and more so near the EDJ (below). These processes become contiguous towards the end of crown formation, as the maturation wave converges with secretion near the cervix (right).

https://doi.org/10.1371/journal.pone.0186391.g008

caused by mineralization disruption [16]. These hypomineralized spots may show frequencies as high as 44% in some human populations [49]. Furthermore, because HAp forms in equilibrium with blood chemistry, a concrete model of mineralization can aid retrospective inferences of environmental toxin exposure, diet, health and behavior from measurements of mature teeth. Measurements of lead or other harmful compounds in teeth can theoretically provide blood concentration levels during exposure, the exposure timing itself, and environmental risk to others similarly exposed. This kind of analysis facilitates an assessment of the overall "exposome" from the neonatal period through tooth formation [10].

An empirical model of molar mineralization will be especially valuable for evaluating the relationship between stable light isotopes and the seasonal dietary, behavioral and environmental factors that produced them. In archaeology and paleontology, repeated samples of tooth carbon stable isotopes have been used to infer seasonal grazing upon wet or arid adapted plants, or foraging of terrestrial or marine resources [5,50–52]. Oxygen isotopes have been sampled to indicate seasonal changes in the evaporative state of ingested water or food sources, of the heat or aridity stress of the subject, and of migratory patterns [26–29,52–54]. Secretory and maturation patterns documented in the current study predict that isotopic or elemental histories should be expressed in spatial patterns that mimic both mineralization phases (Fig 6). This appears to be confirmed by the spatial pattern of tooth $\delta^{13}C$ values in an experimental animal that reflect both secretory and maturation geometries [19,30].

Mineralization also informs elemental and isotopic sampling from archaeological and fossil teeth, which can become powerful tools for understanding the behaviors and diets of past

organisms [8,25]. For example, the timing of secretory deposition can help link strontium isotope ratios that reflect geological provenance to concrete early life migratory patterns [55–57]. As the relationships between barium, strontium, and calcium levels to mineral density are further resolved, their spatial patterns in teeth can ever more reliably indicate dietary and weaning behaviors [8,25,58].

The method outlined here, combining an ontogenetic series of synchrotron-based density measurements into an MCMC modeling framework, can be used to reconstruct biomineralization processes in other complex structures and taxa. This is important since formation processes remain elusive for many biomineralized structures that combine organic and inorganic components [59]. These structures range in scale from bacterial precipitates to bivalve shells and adhesive threads [60–62]. For instance, modeling the growth of silica cell walls deployed as biomaterials in filtration, optics, fabrication and drug delivery could aid in their artificial synthesis [9,63].

Our mineralization model relies upon density estimates and cannot directly assess mineral phase transitions that may also impact biomineralization, isotopic and trace element analyses. These transitions, including that from ACP to HAp, are now thought to be integral to biomineralization processes and have been observed in a several taxa [21–24,64,65]. For instance, in some mollusks teeth and shells develop from amorphous calcium carbonate or iron-chiton composites into aragonite or magnetite mineral [21, 64,65]. Evidence of amorphous calcium phosphate transformation into HAp has recently been found in developing *Mus* teeth, possibly facilitated by a variety of physiological processes [23,47,48,66]. Tests of these transitions using isotopic evidence [24] can be more tractable if supported by a general model of mineral density increase as presented here [5,19,54].

Conclusions

Despite the heterogeneity of maturation among individual teeth, synchrotron μCT data from many individuals and tooth locations results in an overall dynamic model that is highly consistent in secretory and maturation geometry with respect to the EDJ, and in the magnitude of density increases. The dynamic model of mineralization presented here shows that sheep molars mineralize in secretion and maturation waves with distinct spatial orientations that are separated temporally until the end of mineralization. This is consistent the view that mineralization is an ordered process, and possibly conserved among taxa [67]. Density characterization and MCMC sampling can be used to reconstruct mineralization patterns in different skeletal and taxonomic contexts, and may further illuminate the dynamic nature of biomineralization. Finally, efforts to quantitatively reconstruct dietary or environmental histories using chemical measurements will be able to assess the relative contributions of secretory and maturation phases, as well as their expected distribution within mature tissues.

Supporting information

S1 Text. Definitions of terms used. This file contains a list of definitions for terms commonly employed by this manuscript. An associated reference list is provided.
(PDF)

S2 Text. Description of additional methods used in this study. This text provides additional detail on synchrotron mineral density measurement, flattening and standardizing virtual enamel sections, estimating initiation and extension, calcein labeling, model conversion between different tooth types, and MCMC methods for estimating mineral density increase

over time. An associated reference list is provided.
(PDF)

S1 Dataset. Virtual sections of enamel mineral density. Virtual buccal enamel sections extracted from synchrotron scanned tooth volumes at 45μm resolution. Brighter pixels indicate dense, highly mineralized enamel, and darker pixels indicate less dense, poorly mineralized enamel. In file name, day of animal death is indicated first, followed by scan batch (1 or 2), followed by animal ID number. 13μm resolution scans ("hi-res") not used to construct the model are also included.
(ZIP)

S1 File. Mineralization model file. H5PY file holding the mineralization model results derived from synchrotron scans and MCMC sampling. File is best opened by HDFView software. The file contains four data sets: age_mask, ages, locations and pct_min_samples. Age_mask data records where each of the 45 scanned M1s (x-axis) contains or does not contain mineral density data for each of 12,000 pixels locations (y-axis). Age_mask data is binary: the presence of data is recorded by a 1, and absence by a 0. Ages data records the age in days of each of the 45 animals. Locations data records the standardized X and Y tooth coordinates (first and second columns of the x-axis) for each of 12,000 pixels. Pct_min_samples data records model estimated mineral density for all locations over time. This dataset contains three axes, with 100 mineral density % samples (x-axis columns) for each of 12,000 pixels (y-axis rows), over all 45 specimen ages (z-axis pages).
(H5)

S2 File. Dynamic model of mineral density increase. Animation showing mineral density increase described by the mineralization model. Dark blue colors indicate no mineral addition, while warmer colors (light blue, yellow, red) indicate higher rates of mineral deposition. Mineral density increase has been Gaussian blurred for the purposes of visualization, with the standard deviation of the Gaussian set to one pixel in both x and y axes, and 8 days in the z (time) axis.
(MP4)

S3 File. Animation of synchrotron mineral density imaging. Animation showing 3D density data collected from synchrotron imaging of a single first molar. Red colors indicate dense, highly mineralized enamel, and blue colors indicate less dense, poorly mineralized enamel. Visualization produced using VGStudio MAX 3.0 software.
(AVI)

Acknowledgments

We are indebted to Michael Thonney and Mary Smith at the Cornell Sheep project for their careful records, and provision of sheep mandible specimens. We are grateful to Daniel Lieberman and David Pilbeam for their helpful comments on this manuscript. This work was supported by National Science Foundation Grants 1247426 and 0923831, the Wenner-Gren Foundation, the Leakey Foundation, Harvard University, and the European Synchrotron Radiation Facility award EC 1018.

Author Contributions

Conceptualization: Daniel R. Green.

Data curation: Daniel R. Green.

Formal analysis: Daniel R. Green, Gregory M. Green, Albert S. Colman, Paul Tafforeau.

Funding acquisition: Daniel R. Green, Tanya M. Smith.

Investigation: Daniel R. Green, Tanya M. Smith.

Methodology: Daniel R. Green, Gregory M. Green, Albert S. Colman, Paul Tafforeau.

Project administration: Tanya M. Smith.

Resources: Daniel R. Green, Paul Tafforeau, Tanya M. Smith.

Software: Daniel R. Green, Gregory M. Green, Paul Tafforeau.

Supervision: Albert S. Colman, Tanya M. Smith.

Validation: Daniel R. Green, Gregory M. Green, Albert S. Colman, Paul Tafforeau.

Visualization: Daniel R. Green.

Writing – original draft: Daniel R. Green.

Writing – review & editing: Daniel R. Green, Felicitas B. Bidlack, Tanya M. Smith.

References

1. Leeuwenhoeck A. Microscopical Observations of the Structure of Teeth and other Bones: Made and Communicated, in a Letter by Mr. Anthony Leeuwenhoeck. Philosophical Transations. 1677 12:1002–1003.
2. Hillson S. Teeth. Cambridge university press; 2005.
3. Smith TM. Incremental dental development: methods and applications in hominoid evolutionary studies. Journal of Human Evolution. 2008 54:205–224. https://doi.org/10.1016/j.jhevol.2007.09.020 PMID: 18045649
4. Ungar PS. Mammal teeth: origin, evolution, and diversity. JHU Press; 2010.
5. Passey B, Cerling T, Schuster G, Robinson T, Roeder B, Krueger S. Inverse methods for estimating primary input signals from time-averaged isotope profiles. Geochimica et Cosmochimica Acta. 2005 69:4101–4116.
6. Smith T, Tafforeau P. New visions of dental tissue research: Tooth development, chemistry, and structure. Evolutionary Anthropology. 2008 17:213–226.
7. Zazzo A, Bendrey R, Vella D, Moloney AP, Monahan FJ, Schmidt O. Refined sampling strategy for intra-tooth stable isotope analysis of enamel. Geochimica et Cosmochimica Acta. 2012 84:113.
8. Austin C, Smith TM, Bradman A, Hinde K, Joannes-Boyau R, Bishop D et al. Barium distributions in teeth reveal early-life dietary transitions in primates. Nature. 2013 4987453:216–9.
9. Wang J, Xiao Q, Zhou H, Sun P, Li B, Ding D, Chen T. Radiolaria-like silica with radial spines fabricated by a dynamic self-organization. The Journal of Physical Chemistry C. 2007 111(44):16544–8.
10. Andra SS, Austin C, Wright RO, Arora M. Reconstructing pre-natal and early childhood exposure to multi-class organic chemicals using teeth: Towards a retrospective temporal exposome. Environmental International. 2015 83:137–145.
11. Kohn M, Cerling TE. Stable Isotope Compositions of Biological Apatite. Reviews in Minerology and Geochemistry. 2002 48:455–488.
12. Diekwisch TG. Subunit compartments of secretory stage enamel matrix. Connective Tissue Research. 1998 38:101–11. PMID: 11063019
13. Smith CE. Cellular and Chemical Events During Enamel Maturation. Critical Reviews in Oral and Biological Medicine. 1998 9:128–161.
14. Lacruz RS, Habelitz S, Wright JT, Paine ML. Dental enamel formation and implications for oral health and disease. Physiological Reviews. 2017 97:939–993. https://doi.org/10.1152/physrev.00030.2016 PMID: 28468833
15. Suga S. Progressive mineralization pattern of developing enamel during the maturation stage. Journal of Dental Research. 1982 1532–1542. PMID: 6958712
16. Suga S. Enamel hypomineralization viewed from the pattern of progressive mineralization of human and monkey developing enamel. Journal of Dental Research. 1989 32:188–198.

17. Passey BH, Cerling TE. Tooth enamel mineralization in ungulates: implications for recovering a primary isotopic time-series. Geochimica et Cosmochimica Acta. 2002 66:3225–3234.
18. Hoppe KA, Stover SM, Pascoe JR, Amundson R. Tooth biomineralization in horses: implications for isotopic microsampling. Palaeogeography Palaeoclimatology Palaeoecology. 2004 206:355–365.
19. Trayler RB and Kohn MJ. Tooth enamel maturation reequilibrates oxygen isotope compositions and supports simple sampling methods. Geochimica et Cosmochimica Acta. 2017 198:32–47.
20. Chai H, Lee JJ, Constantino PJ, Lucas PW, Lawn BR. Remarkable resilience of teeth. Proceedings of the National Academy of Sciences. 2009 106(18):7289–93.
21. Wang Q, Nemoto M, Li D, Weaver JC, Weden B, Stegemeier J et al. Phase transformations and structural developments in the radular teeth of Cryptochiton stelleri. Advanced Functional Materials. 2013 2323:2908–17.
22. Weaver JC, Wang Q, Miserez A, Tantuccio A, Stromberg R, Bozhilov KN, et al. Analysis of an ultra hard magnetic biomineral in chiton radular teeth. Materials Today. 2010 13(1):42–52.
23. Beniash E, Metzler RA, Lam RSK, Gilbert P. Transient amorphous calcium phosphate in forming enamel. Journal Structure Biology. 2009 166:133–143.
24. De Yoreo JJ, Gilbert PUPA, Sommerdijk NAJM, Lee Penn R, Whitelam S, Joester D et al. Crystallization by particle attachment in synthetic, biogenic, geologic environments. Science. 2015 349(6247): aaa6760. https://doi.org/10.1126/science.aaa6760 PMID: 26228157
25. Humphrey LT. Isotopic and trace element evidence of dietary transitions in early life. Annals of Human Biology. 2014 414:348–57.
26. Nelson SV. Isotopic reconstructions of habitat change surrounding the extinction of Sivapithecus, a Miocene hominoid, in the Siwalik Group of Pakistan. Palaeogeography, Palaeoclimatology, Palaeoecology. 2007 Jan 10; 243(1):204–22.
27. Kirsanow K, Makarewicz C, Tuross N. Stable oxygen δ18O and hydrogen δD isotopes in ovicaprid dentinal collagen record seasonal variation. Journal of Archaeological Science. 2008 3512:3159–67.
28. Fricke HC, Hencecroth J, Hoerner ME. Lowland–upland migration of sauropod dinosaurs during the Late Jurassic epoch. Nature. 2011 10570.
29. Balasse M, Obein G, Ughetto-Monfrin J, Mainland I. Investigating seasonality, birth in herds: a reference set of sheep enamel stable oxygen isotope ratios. Archaeometry. 2012 54:349.
30. Zazzo A, Balasse M, Patterson WP. High-resolution δ 13 C intratooth profiles in bovine enamel: Implications for mineralization pattern and isotopic attenuation. Geochimica et Cosmochimica Acta. 2005 69(14):3631–42.
31. Simmer J, Richardson A, Hu Y-Y, Smith C, Hu J. A post-classical theory of enamel biomineralization. . . and why we need one. International Journal of Oral Science. 2012 4:129–134. https://doi.org/10.1038/ijos.2012.59 PMID: 22996272
32. Boyde A. Enamel. In Teeth 309–473. 2009 Springer Berlin Heidelberg.
33. Smith TM. Experimental determination of the periodicity of incremental features in enamel. Journal of Anatomy. 2006 208:99–113. https://doi.org/10.1111/j.1469-7580.2006.00499.x PMID: 16420383
34. Tafforeau P, Bentaleb I, Jaeger JJ, Martin C. Nature of laminations and mineralization in rhinoceros enamel using histology and X-ray synchrotron microtomography. Palaeogeography Palaeoclimatology Palaeoecology. 2007 246:206–227.
35. Fukae M, Yamamoto R, Karakida T, Shimoda S, Tanabe T. Micelle structure of amelogenin in porcine secretory enamel. Journal of dental research. 2007 Aug; 86(8):758–63. https://doi.org/10.1177/154405910708600814 PMID: 17652206
36. Driessens F, Verbeeck RK. Biominerals. 1990 CRC Press.
37. Zazzo A, Balasse M, Passey B, Moloney A, Monahan F, Schmidt O. The isotope record of short- and long-term dietary changes in sheep tooth enamel: Implications for quantitative reconstruction of paleodiets. Geochimica et Cosmochimica Acta. 2010 74:3571–3586.
38. Blumenthal S, Cerling T, Chritz K, Bromage TG, Kozdon R, Valley JW. Stable isotope time-series in mammalian teeth: In situ δ18O from the innermost enamel layer. Geochimica et Cosmochimica Acta. 2014 124:223236.
39. Zou W, Gao J, Jones AS, Hunter N, Swain MV. Characterization of a novel calibration method for mineral density determination of dentine by X-ray micro-tomography. Analyst. 2009; 134(1):72–9. https://doi.org/10.1039/b806884d PMID: 19082177
40. Zou W, Hunter N, Swain MV. Application of polychromatic μCT for mineral density determination. Journal of dental research. 2011; 90(1):18–30. https://doi.org/10.1177/0022034510378429 PMID: 20858779

41. Nuzzo S, Peyrin F, Cloetens P, Baruchel J, Boivin G. Quantification of the degree of mineralization of bone in three dimensions using synchrotron radiation microtomography. Medical Physics. 2002 29:2672–2681. https://doi.org/10.1118/1.1513161 PMID: 12462734

42. Jordana X, Köhler M. Enamel microstructure in the fossil bovid Myotragus balearicus Majorca, Spain: implications for life-history evolution of dwarf mammals in insular ecosystems. Palaeogeography Palaeoclimatology Palaeoecology. 2011 300:59–66.

43. Kierdorf H, Kierdorf U, Frölich K, Witzel C. Lines of Evidence–Incremental Markings in Molar Enamel of Soay Sheep Revealed by Fluorochrome Labeling, Backscattered Electron Imaging Study. PLOS ONE. 2013 8.9:e74597. https://doi.org/10.1371/journal.pone.0074597 PMID: 24040293

44. Powell MJD. Direct search algorithms for optimization calculations. Acta Numerica. 1998 7:287–336.

45. Kucherenko S, Sytsko Y. Application of deterministic low-discrepancy sequences in global optimization. Computational Optimization and Applications. 2005 30:297–318.

46. Bendrey R, Vella D, Zazzo A, Balasse M, Lepetz S. Exponentially decreasing tooth growth rate in horse teeth: implications for isotopic analyses. Archaeometry. 2015 57(6):1104–24.

47. Josephsen K, Takano Y, Frische S, Praetorius J, Nielsen S, Aoba T, Fejerskov O. Ion transporters in secretory and cyclically modulating ameloblasts: a new hypothesis for cellular control of preeruptive enamel maturation. American Journal of Physiology Cell Physiology. 2010 299:C1299–307. https://doi.org/10.1152/ajpcell.00218.2010 PMID: 20844245

48. Damkier HH, Josephsen K, Takano Y, Zahn D, Fejerskov O, Frische S. Fluctuations in surface pH of maturing rat incisor enamel are a result of cycles of H+-secretion by ameloblasts and variations in enamel buffer characteristics. Bone. 2014 60:227–34. https://doi.org/10.1016/j.bone.2013.12.018 PMID: 24373736

49. Jälevik B. Prevalence and diagnosis of molar-incisor-hypomineralisation MIH: a systematic review. European Archives of Paediatric Dentistry. 2010 112:59–64.

50. Sponheimer M, Passey B H, de Ruiter D J, Guatelli-Steinberg D, Cerling TE, Lee-Thorp JA. Isotopic Evidence for Dietary Variability in the Early Hominin P. robustus. Science. 2006 314:980–982. https://doi.org/10.1126/science.1133827 PMID: 17095699

51. Eerkens JW, Sullivan K, Greenwald AM. Stable isotope analysis of serial samples of third molars as insight into inter-and intra-individual variation in ancient diet. Journal of Archaeological Science Reports. 2016 5:656–63.

52. Lüdecke T, Mulch A, Kullmer O, Sandrock O, Thiemeyer H, Fiebig J, Schrenk F. Stable isotope dietary reconstructions of herbivore enamel reveal heterogeneous savanna ecosystems in the Plio-Pleistocene Malawi Rift. Palaeogeography, Palaeoclimatology, Palaeoecology. 2016 Oct 1; 459:170–81.

53. Gat J. Oxygen and hydrogen isotopes in the hydrologic cycle. Annual Reviews in Earth and Planetary Science. 1996 24:225262.

54. Green DR. Reconstructing oxygen isotope seasonality in large herbivores through mineralization modeling, experimentation and optimization. Doctoral Dissertation. Harvard University. 2016.

55. Richards M, Harvati K, Grimes V, Smith C, Smith T, Hublin J-J et al. Strontium isotope evidence of Neanderthal mobility at the site of Lakonis, Greece using laser-ablation PIMMS. Journal of Archaeological Science. 2008 355:1251–6.

56. Britton K, Grimes V, Dau J, Richards MP. Reconstructing faunal migrations using intra-tooth sampling and strontium and oxygen isotope analyses: a case study of modern caribou Rangifer tarandus granti. Journal Archaeological Science. 2009 365:1163–72.

57. Copeland SR, Cawthra HC, Fisher EC, Lee-Thorp JA, Cowling RM, le Roux PJ et al. Strontium isotope investigation of ungulate movement patterns on the Pleistocene Paleo-Agulhas Plain of the Greater Cape Floristic Region, South Africa. Quaternary Science Reviews. 2016 141:65–84.

58. Smith TM, Austin C, Hinde K, Vogel ER, Arora M. Cyclical nursing patterns in wild orangutans. Science Advances. 2017 3:e1601517–1–8. https://doi.org/10.1126/sciadv.1601517 PMID: 28560319

59. Cölfen H. A crystal-clear view. Nature Materials. 2010 9:960–961. https://doi.org/10.1038/nmat2911 PMID: 21102512

60. Ehrlich H. Chitin and collagen as universal and alternative templates in biomineralization. International Geology Review. 2010 52(7–8):661–99.

61. Guerette PA, Hoon S, Seow Y, Raida M, Masic A, Wong FT, et al. Accelerating the design of biomimetic materials by integrating RNA-seq with proteomics and materials science. Nature biotechnology. 2013 31(10):908–15. https://doi.org/10.1038/nbt.2671 PMID: 24013196

62. Green DW, Lee JM, Jung HS. Marine structural biomaterials in medical biomimicry. Tissue Engineering Part B: Reviews. 2015 21(5):438–50.

63. Aw MS, Simovic S, Addai-Mensah J, Losic D. Silica microcapsules from diatoms as new carrier for delivery of therapeutics. Nanomedicine. 2011 6(7):1159–73. https://doi.org/10.2217/nnm.11.29 PMID: 21707299

64. Gong YU, Killian CE, Olson IC, Appathurai NP, Amasino AL, Martin MC, et al. Phase transitions in biogenic amorphous calcium carbonate. Proceedings of the National Academy of Science. 2012 10916:6088–93.

65. DeVol RT, Sun CY, Marcus MA, Coppersmith SN, Myneni SC, Gilbert PU. Nanoscale transforming mineral phases in fresh nacre. Journal of the American Chemical Society. 2015 13741:13325–33.

66. Kallistová A, Horáček I, Šlouf M, Skála R, Fridrichová M. Mammalian enamel maturation: Crystallographic changes prior to tooth eruption. PloS one. 2017 12(2):e0171424. https://doi.org/10.1371/journal.pone.0171424 PMID: 28196135

67. Fraser GJ, Hulsey CD, Bloomquist RF, Uyesugi K, Manley NR, Streelman JT. An ancient gene network is co-opted for teeth on old and new jaws. PLoS Biol. 2009 7(2):e1000031.